

# IMPEDANCE OPTIMIZATION OF SIRIUS STRIPLINE KICKER

H.O.C. Duarte\*, S.R. Marques, LNLS, Campinas, Brazil

## Abstract

Two approaches to design a transverse feedback (TFB) stripline kicker are well known in the accelerators community: one with bare strips in a tapered cavity and other whose shrouded strips are ended with parallel-plate capacitive gaps. This work presents a comparison between both models in terms of electromagnetic performance, proposes alternative solutions for increasing the gap capacitance and analyzes the performance of a hybrid stripline kicker design.

## INTRODUCTION

Studies of collective beam instabilities for Sirius, the 3 GeV light source under construction in Brazil [1], have shown the need of the transverse bunch-by-bunch (BBB) feedback system in the storage ring since day one [2]. For the longitudinal plane, at least for the initial phases, the use of BBB feedback system is not planned since superconducting RF cavities will be used.

The digital signal processing for the BBB system will be performed by the front/back-end and iGp processor units from Dimtel, Inc. [3] and the actuators will be one  $\lambda/2$  stripline kicker for each plane. A  $\lambda/4$  stripline tune monitor is also planned.

This contribution describes the evolution of the stripline kicker design for Sirius. At first, several concepts were tested regarding their transverse geometric factor and longitudinal coupling impedance. Then the best suited geometry was optimized following the compromise between the reflection parameter at the input coaxial ports and the geometric loss factor of the structure. Shunt impedance was also evaluated and finally the mechanical project and thermal simulation results are shown.

## GEOMETRY ALTERNATIVES

The electromagnetic design evolution for Sirius stripline kicker was carried out by analysing three different concepts to further optimize the longitudinal impedance spectrum and the reflection parameters of the chosen one. GdfidL [4] was used for the electromagnetic simulations.

### Transverse 2D Analysis

All presented stripline geometries can be grouped in either of these two transverse profiles: Bare Strip and Shrouded Strip designs, whose dimensions are shown in Fig. 1. While solving the 2D Laplace's equation for an electric boundary condition (BC) characterizes the odd mode, which is the kicker operation mode, the solution for a magnetic BC would give the field distribution for the even mode [5]. Both profiles in Fig. 1 had their geometry parameters set to match a 50  $\Omega$

characteristic impedance (i.e., 25  $\Omega$  for the full structure containing two electrodes). An impedance mismatching can impact the beam coupling impedance [6] and the port signal reflection.

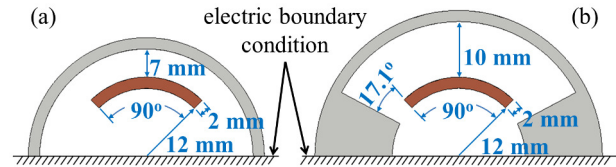


Figure 1: The considered transverse profiles for the vertical striplines: a) Bare Strip and b) Shrouded Strip designs.

From the mentioned 2D electrostatic analysis one can also determine the transverse geometric factor  $g_{\perp}$ . For the Bare Strip (Fig. 1a) and Shrouded Strip designs (Fig. 1b),  $g_{\perp}$  is equal to 1.09 and 1.01 respectively. The geometric factor allows determining the transverse beam impedance [5]:

$$Z_{\perp}(k) = \frac{g_{\perp}^2 Z_{ch,\perp}}{kr^2} [\sin^2(kL) + j \sin(kL) \cos(kL)] \quad (1)$$

where  $k$  is the wave number,  $Z_{ch,\perp}$  the full structure characteristic impedance for the odd mode (25  $\Omega$ ),  $r$  the stripline inner radius (12 mm) and  $L$  the stripline length, which determines the kicker operation bandwidth (BW). Choosing  $L = \lambda/2 = 30$  cm provides 250 MHz shunt impedance BW [7], which is enough for correcting Sirius transverse coupled-bunch instabilities (CBMIs) [8] since Sirius RF frequency is  $\sim 500$  MHz. The shunt impedance can be calculated by [5]

$$R_{sh}^{\perp} = \frac{4 \times \Re Z_{\perp}(k)}{k} \quad (2)$$

For a kicker, the shunt impedance is an important parameter since it quantifies its efficiency relating the injected power with the kick energy absorbed by the beam. Given that both transverse profiles in Fig. 1 only differ by the geometric factor, it is straightforward to see in Eq. 1 that a transverse kicker with Bare Strip transverse profile is 16.5% more efficient than one with the Shrouded Strip design type. However, the stripline ends affect other aspects of the kicker and a three-dimensional analysis must be performed for a satisfactory characterization.

### Longitudinal 3D Analysis

Figure 2 shows the simplified geometries for the simulation models of three different stripline concepts. The Tapered Cavity Stripline is the design approach considered by NSLS-II [9]. Its adapted model consists of bare strips (see Fig. 1a) placed inside a 1/15 linearly tapered cavity that reaches the 24 mm diameter vacuum chamber profile

\* henrique.caiafa@lnls.br

on both ends. Another design type, the Capacitive Gap, which was inspired by SOLEIL stripline [10], consists of shrouded strips (see Fig. 1b) with 0.5 mm capacitive gaps at both ends and thus following the vacuum chamber profile. Based on these two approaches, a hybrid design was also simulated and considered for comparison. It consists of the Bare Strip transverse profile with the stripline ended by capacitive gaps whose capacitance was set to keep the same as of the Capacitive Gap type. The chamber transitions follow the 24 mm diameter round profile in the vertical plane (limited by the 90° stripline aperture angle) but a 1/15 tapered transition, that finally reaches the vacuum chamber profile, is found in the horizontal plane.

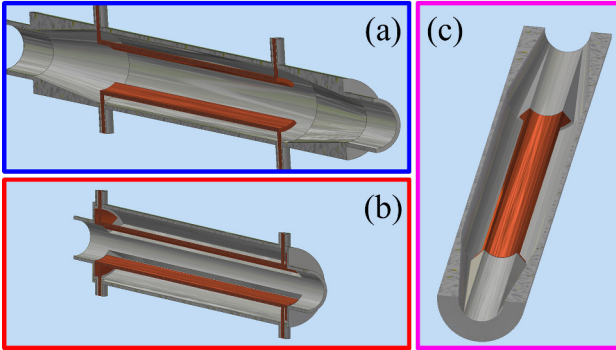


Figure 2: Analysed stripline approaches: a) Left half of the Tapered Cavity type. b) Right half of the Capacitive Gap type. c) Bottom half of the Hybrid type.

Figure 3 compares the real part of longitudinal beam impedance of the three discussed design approaches. The Tapered Cavity design shows higher broadband impedance than the other two geometries. Its lower frequency portion, below 17 GHz, is most impacted by the bare ends of the stripline, because the spectrum of the power sum signal of the feedthrough ports approximately matches the impedance within this frequency range. On the other hand, the energy lost by the beam caused by the tapered cavity shape, flows through the beam ports and impacts the high frequency part of the impedance [9]. One can also notice the gap capacitance effect for both Hybrid and Capacitive Gap geometries, where the feedthrough output signals start to be filtered out right above 500 MHz, although stronger HOMs are generated.

To allow further comparison, the geometric single-bunch (SB) and multi-bunch (MB) loss factors were evaluated for the simulated bunch length  $\sigma_s = 2.65$  mm and the 3.8 mm length expected for Sirius Phase 1 [11]. Their values are shown in Table 1.

Table 1: Geometric SB and MB Loss Factor Comparison among Tapered Cavity, Capacitive Gap and Hybrid Stripline Types for Two Bunch Length Scenarios

Geometry type	Geometric $\kappa_{loss}$ , mV/pC			
	$\sigma_s = 2.65$ mm		$\sigma_s = 3.8$ mm	
	SB	MB	SB	MB
Tapered Cavity	614.7	559.7	423.9	361.6
Capacitive Gap	74.9	43.2	48.5	21.8
Hybrid	131.2	75.3	84.9	40.6

Both SB and MB loss factors were evaluated from the impedance spectra presented in Fig. 3 through the Eqs. 3 and 4, respectively [12, 13]. For the later, a uniform filling pattern is considered.

$$\begin{aligned} \kappa_{loss}^{SB} &= \frac{\omega_0}{\pi} \sum_{p=1}^{\infty} \Re Z_{\parallel}(p\omega_0) e^{-(p\omega_0\sigma_s/c)^2} \\ &\approx \frac{1}{\pi} \int_0^{\infty} \Re Z_{\parallel}(\omega) e^{-(\omega\sigma_s/c)^2} d\omega \end{aligned} \quad (3)$$

$$\kappa_{loss}^{MB} = \frac{M\omega_0}{\pi} \sum_{p=1}^{\infty} \Re Z_{\parallel}(pM\omega_0) e^{-(pM\omega_0\sigma_s/c)^2} \quad (4)$$

where  $c$  is the speed of light,  $M = 864$  is the harmonic number and  $\omega_0 = 3.634$  Mrad/s the revolution frequency of Sirius storage ring.

As can be seen in Table 1, all MB loss factors were smaller than the SB ones, since no strong HOM was sampled in the impedance spectra and local minima at RF frequency multiples (i.e.,  $pM\omega_0$ ) are found below 4 GHz. Despite having stronger HOMs and 16.5% lower shunt impedance due to the Shrouded Strip transverse profile, the Capacitive Gap geometry was preferred since its beam load is  $\sim 2$  and  $\sim 15$  times weaker than the Hybrid and Tapered Cavity types, respectively.

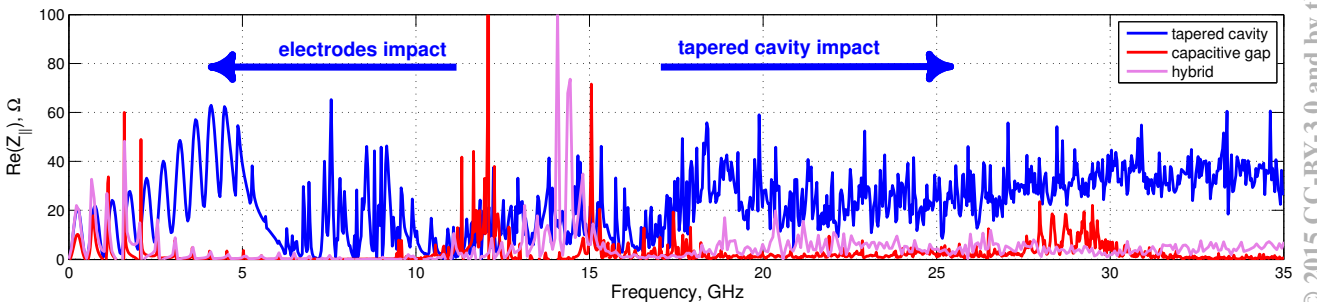


Figure 3: Real part of longitudinal beam impedance of the Tapered Cavity, Capacitive Gap and Hybrid stripline geometries.

### CAPACITIVE GAP ALTERNATIVES

After selecting the Capacitive Gap geometry type, the idea of studying alternative gap types was welcomed not only for increasing the gap capacitance, but also for allowing alternative mechanical solutions for expected thermal expansions. Therefore, besides the previously analysed Standard Gap type, three gap geometries were proposed: Sliding Gap, Upper Gap and Comb-type Gap, as shown in Fig. 4 below:

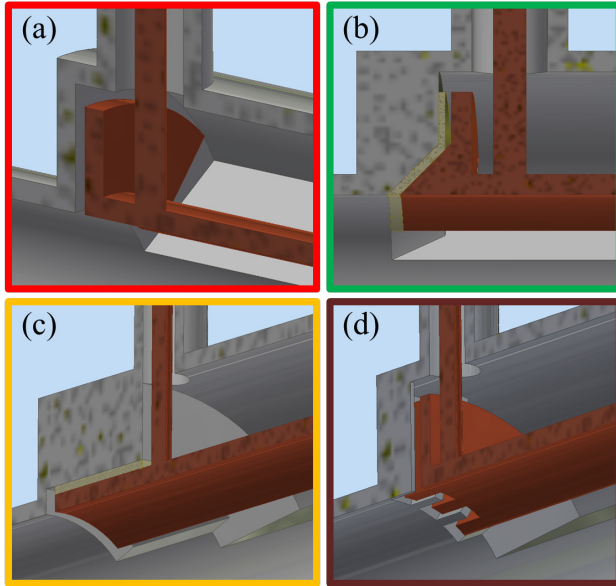


Figure 4: Considered capacitive gap types: a) Standard Gap b) Sliding Gap c) Upper Gap d) Comb-type Gap.

The previously analysed Standard Gap is a 0.5 mm gap transverse to the beam axis. For the Sliding Gap this size is 1 mm, filled by a 0.5 mm thick alumina insulator that lies in the 45° and 5 mm chamfered transverse wall of the cavity. Such slope turns any longitudinal expansion of the stripline into a transverse motion. The Upper Gap type contains a 20 mm length and 1 mm thick ceramic slit that touches the upper face of the stripline end, which has a 2 mm longitudinal clearance. Finally, as shown in Fig. 5, the Comb-type Gap, inspired by the RF shielding for KEK bellows and gate valves [14], consists of 5 mm length ( $a$  parameter) nested teeth whose

parallel side faces are separated by a 0.5 mm gap  $b$  and the front faces by a longitudinal gap  $c$  of 2 mm. For Standard and Sliding Gap types as well, the plates, whose 10 mm height also follows  $d$  from Fig. 5, stay radially 2 mm away from the cavity wall.

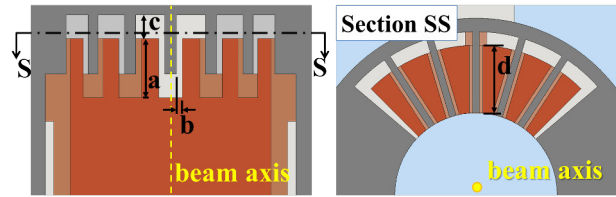


Figure 5: Comb-type Gap geometry parameters. Left: beam/bottom view. Right: Transverse cut (Section SS) view.

Figure 6 shows the real part of the longitudinal impedance of the four capacitive gap striplines and the correspondent SB and MB loss factors are found at Table 2. Due to the highest wake losses, the Upper Gap design was discarded. Among the remaining three, the Standard Gap type was the least desired as a gap size lower than 0.5 mm was not acceptable, considering the risk of short-circuiting the gap by thermal expansions and/or mechanical tolerances. Finally, since the Sliding Gap requires a complex three-dimensional ceramic slit due to the chamfer in the round edge cavity profile, the Comb-type was preferred even though its MB loss factor gets higher than the SB one. This occurs because three HOMs are sampled by RF multiples.

Table 2: Geometric SB and MB Loss Factors of the Standard, Sliding, Upper and Comb-type Gaps for Two Bunch Length Scenarios

Geometry type	Geometric $\kappa_{loss}$ , mV/pC			
	$\sigma_s = 2.65$ mm		$\sigma_s = 3.8$ mm	
	SB	MB	SB	MB
Upper	202.0	185.5	94.7	79.5
Standard	74.9	43.2	48.5	21.8
Sliding	45.2	17.4	30.8	8.2
Comb-type	35.5	40.0	24.6	23.7

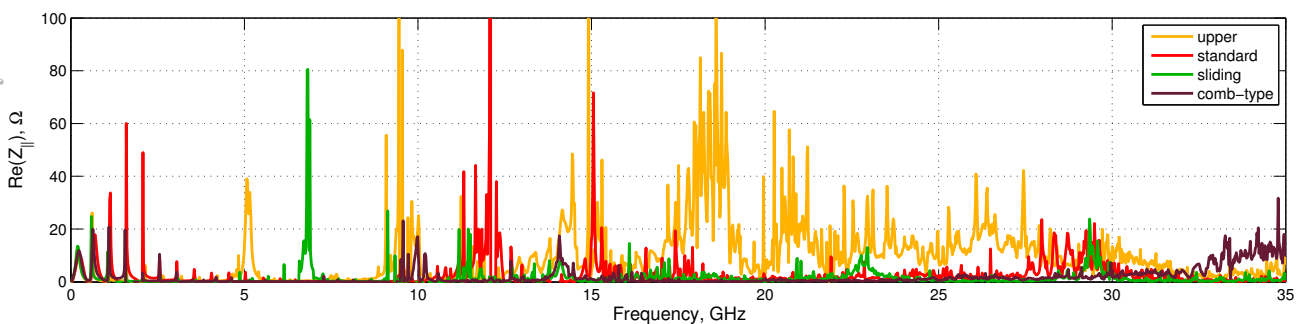


Figure 6: Comparison between the real part of longitudinal beam impedance of the Standard, Sliding, Upper and Comb-type Capacitive Gap striplines.

## S1,1 OPTIMIZATION

For the the initial S-Parameter analysis, a pin holder was included, whose design, shown in Fig. 7, was proposed from the idea of allowing longitudinal offsets between the stripline and the pin through elastic deformation of its 0.3 mm thick slits, without stressing the feedthrough ceramic insulator. Although the holder was included in the simulation models, the feedthrough ceramic insulators were not considered since the use of commercial components is planned.

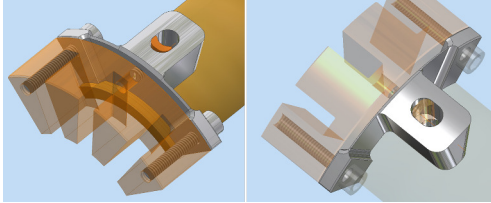


Figure 7: Mechanical design of the pin holder.

The first analysis have shown that the Comb-type gap capacitance was too high for a satisfactory reflection at the input coaxial port (S1,1) within the 250 MHz operation BW, showing a -12 dB (25%) maximum. A -16.5 dB (15%) goal was set to provide a good balance between signal distortion and wake losses, since reducing the mentioned capacitance increases the beam power outgoing the feedthroughs.

The S1,1 optimization shown in Fig. 8 can be separated into two stages. In the first one, a rectangular waveguide (WG), centered with the pin, was inserted between the coaxial line and the gap teeth in order to add an inductive component for compensating the gap capacitance, but was not enough for achieving the desired goal. In the second stage, as depicted by Fig. 9, two alternative geometries for reducing the the gap capacitance have been designed: Geometry 1 has the gap between teeth ( $b$  from Fig. 5) equal to 0.7 mm and the lateral gaps increased as much as possible; Geometry 2 has 4 teeth instead of 6 and kept the geometry parameters  $a-d$  to their original values. Both geometries have reached -16.4 dB maximum within the 250 MHz BW.

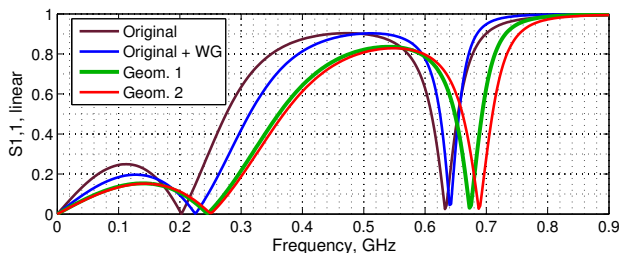


Figure 8: Optimization stages of the S1,1 parameter for the comb-type gap stripline.

Although good equivalence in the S1,1-parameters performance was found for both geometries, Geometry 2 was preferred as it drains lower beam load than Geometry 1. The SB and MB loss factors from the former were 55.15 mV/pC and 42.91 mV/pC, respectively, while the later achieved 29% and 84% higher corresponding values.

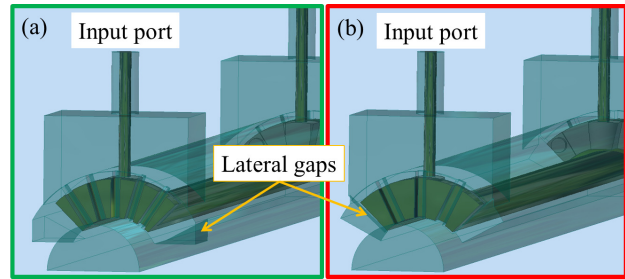


Figure 9: Vacuum profile of the geometry alternatives to reduce the gap capacitance: a) Geometry 1 b) Geometry 2.

## TRANSVERSE SHUNT IMPEDANCE

The vertical coupling impedances for Geometry 2 and original Comb-type Gap design were simulated and their shunt impedances obtained by Eq. 2. In Fig. 10, the results are compared with the one calculated from Eqs. 1 and 2 and good agreement was found. The gap capacitance interferes with the shunt impedance frequency response by distorting the symmetry of the vertical impedance's fundamental mode.

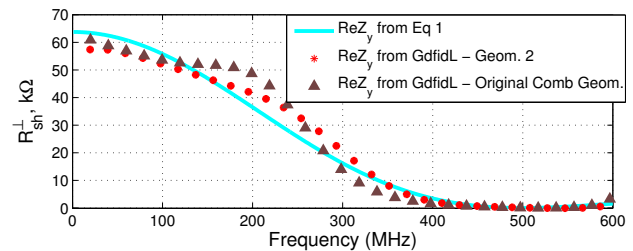


Figure 10: Vertical shunt impedance for Geometry 2 and original design, compared with the one from Eqs. 1 and 2.

## THERMO-MECHANICAL ANALYSIS

The power dissipated in the structure by Joule effect can be obtained by two different approaches. The first is taking the difference between the resistive-wall  $\kappa_{loss,RW}^{MB}$  and the geometric  $\kappa_{loss,geom}^{MB}$  loss factors:

$$P_{loss} = \frac{2\pi}{M\omega_0} (\kappa_{loss,RW}^{MB} - \kappa_{loss,geom}^{MB}) I_{av}^2 \quad (5)$$

where  $I_{av}$  is the beam average current. The second approach is subtracting the coaxial and beam ports output power from the  $\kappa_{loss,RW}^{MB}$  total power loss alone [15]. In the following analysis the first method was employed, but both of them give similar results.

The difference between RW and geometric loss factors is 11.71 mV/pC for Geometry 2, considering 2.65 mm bunch length. Assuming 500 mA average current as a worst case scenario, Eq. 5 provides  $P_{loss} = 5.86$  W. Twice this input power was considered and distributed, according to GdfidL result, among the geometry parts as shown by Table 3 in the thermal simulation model. Electrical conductivities for Copper and Stainless Steel were considered as  $5.80 \times 10^7$  S/m and  $1.43 \times 10^6$  S/m respectively.

Table 3: Power Loss Distribution among the Geometry Parts

Component	Material	Power %	Power, W
Cav. + end pipes	SS	33.17	3.888
Cavity ridges	SS	39.97	4.685
WG + outer coax.	SS	2.91	0.341
Stripline (SL)	Cu	8.57	1.004
SL teeth	Cu	1.48	0.173
Chamber Teeth	SS	10.85	1.271
Feedthrough pins	SS	1.04	0.122
Holder slits	SS	0.53	0.062
Holder-center	SS	1.01	0.118
Holder-sides	SS	0.47	0.055

Figure 11 depicts the mechanical design used in the thermo-mechanical simulation shown in Fig. 12. Two alumina insulators were considered: a tiny saddle-shaped ceramic spacer, to avoid short-circuiting the gap and a 5 mm thick washer in the feedthrough for holding its pin. Thermal analysis have shown the stripline center and the pin holder as the hottest spots, reaching temperatures up to 50°C and a 9°C gradient was found along the pin. Mechanical results provides only 20  $\mu\text{m}$  longitudinal gap contraction and also shows that the holder was not optimized to avoid the pin bending. Even though the consequent von Mises equivalent stress over the ceramics feedthrough is 80 MPa, much below the ceramics breaking point, modifications in the geometry and material of the pin holder will be analysed in order to reduce the stresses at the feedthrough.

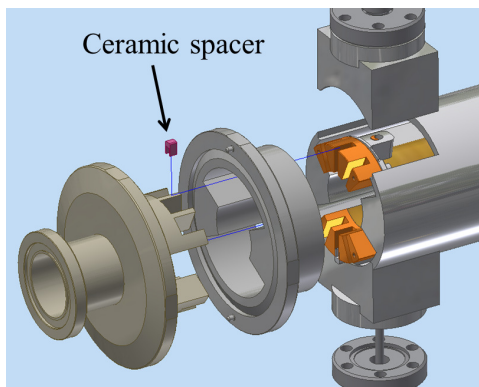
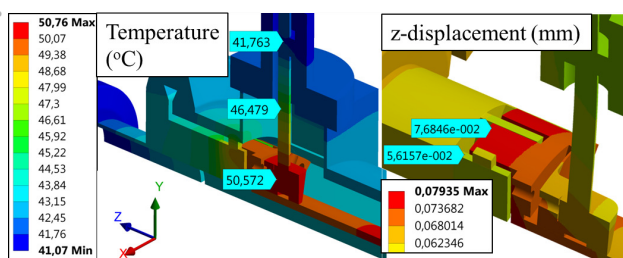


Figure 11: Mechanical design of the stripline kicker.

Figure 12: Thermal (left) and mechanical (right) simulation. On the later, 80 $\times$  distortion magnification is shown.

## CONCLUSION

The stripline kicker Comb-type gap stripline choice and its optimized Geometry 2 were shown by this work. The comb-type gap design have helped reducing wake heating in the components and beam load outgoing the feedthroughs. However, a HOM analysis in frequency domain is desirable for improving the accuracy of such wake heating evaluation. The first kicker prototype is scheduled for late this year.

## ACKNOWLEDGMENT

The authors would like to thank not only Thiago M. Rocha (from LNLS Vacuum Group) for his tremendous support and execution of the mechanical design and thermal simulations, but also E. Plouviez, G. Rehm, A. Morgan and J.J. Sebek for the fruitful discussions. Last but not least, special thanks must go to SINAPAD [16] colleagues for the clusters infrastructure and their excellent technical support.

## REFERENCES

- [1] A.R.D. Rodrigues et al., "Sirius Accelerators Status Report", TUPWA006, Proc. IPAC2015, May 2015.
- [2] F.H. Sá et al., "Study of Collective Beam Instabilities for Sirius", TUPRI041, Proc. IPAC2014, June 2014.
- [3] Dimtel, Inc., <http://www.dimtel.com>
- [4] W. Bruns, GdfidL, <http://www.gdfid1.de>
- [5] D. A. Goldberg and G. R. Lambertson, "Dynamic Devices – A Primer on Pickups and Kickers" LBL-31664, Nov. 1991.
- [6] A. Blednykh et al., "Stripline Beam Impedance", WEPBA06, Proc. PAC2013, September 2014.
- [7] M. Schedler et al., "A Broadband RF Stripline Kicker for Damping Transversal Multibunch Instabilities", MOPO003, Proc. IPAC2011, September 2011.
- [8] M. Lonza, "Digital signal Processing – Multi-bunch feedback systems", CERN Accelerator School, May 2007.
- [9] A. Blednykh, "Beam Impedance and Heating for Several Important NSLS-II Components", Mini-Workshop, DIAMOND, January, 2013.
- [10] C. Mariette et al., "Excitation Stripline for SOLEIL Fast Transverse Feedback", WEPC16, Proc. DIPAC 2007, May 2007.
- [11] L. Liu et al., "Update on Sirius, The New Brazilian Light Source", MOPRO048, Proc. IPAC2014, June 2014.
- [12] B.W. Zotter and S.A. Kheifets, *Impedances and Wakes in High-Energy Particle Accelerators*, ISBN: 9810226268, World Scientific, Singapore (1997), pp. 98-99.
- [13] M. Furman et al., "Energy Loss of Bunched Beams in SSC RF Cavities", SSC-116, Proc. PAC1987, March 1987.
- [14] Y. Suetsugu et al., "Application of Comb-type RF-shield to Bellows Chambers and Gate Valves", RPPE052, Proc. PAC2005, May 2005.
- [15] A. Morgan and G. Rehm, "Finding the Thermal Distribution of Wake Losses", Mini-Workshop, DIAMOND, January, 2013.
- [16] SINAPAD, <https://www.lncc.br/sinapad/>